NIH RELAIS Document Delivery

NIH-10286760

JEFFDUYN

NIH -- W1 JO595L

JOZEF DUYN
10 Center Dirve
Bldg. 10/Rm.1L07
Bethesda, MD 20892-1150

ATTN:
PHONE: 301-594-7305
FAX: -
E-MAIL:

SUBMITTED: 2002-08-29 17:22:18
PRINTED: 2002-09-03 06:21:51
REQUEST NO.:NIH-10286760
SENT VIA: LOAN DOC
7967422

NIH Fiche to Paper Journal

TITLE: JOURNAL OF COMPUTER ASSISTED TOMOGRAPHY
PUBLISHER/PLACE: Lippincott Williams _Wilkins, Hagerstown, MD :
VOLUME/ISSUE/PAGES:1994 Sep-Oct;18(5):697-704 697-704
DATE: 1994
AUTHOR OF ARTICLE: Fulham MJ; Dietz MJ; Duyn JH; Shih HH; Alger JR; Di Chiro G
TITLE OF ARTICLE: Transsynaptic reduction in N-acetyl-aspartate in c
ISSN: 0363-8715
OTHER NOS/LETTERS: Library reports holding volume or year
7703942
8089315
SOURCE: PubMed
CALL NUMBER: W1 JO595L
REQUESTER INFO: JEFFDUYN
DELIVERY: E-mail: jhd@helix.nih.gov
REPLY: Mail:

Journal of Computer Assisted Tomography
18(5):697–704, September/October

Transsynaptic Reduction in N-Acetyl-Aspartate in Cerebellar Diaschisis: A Proton MR Spectroscopic Imaging Study

Michael J. Fulham, Mark J. Dietz, Jeff H. Duyn, Henry H.-L. Shih, Jeffry R. Alger, and Giovanni Di Chiro

Objective: To determine if the transneuronal cerebellar hemispheric metabolic asymmetry seen in crossed cerebellar diaschisis, and readily detected with positron emission tomography (PET), is associated with alterations in metabolite signal intensities on [^{1}H]MR spectroscopic (MRS) imaging when compared with the normal pattern and distribution of cerebellar metabolites.

Materials and Methods: The pattern and distribution of metabolites [N-acetyl-aspartate (NAA), choline-containing compounds, creatine, phosphocreatine, and lactate] in the cerebellum, using [^{1}H]MRS imaging, were studied in a patient with documented long-standing (3 years duration) crossed cerebellar diaschisis and seven normal subjects. Cerebellar diaschisis was detected with fluorodeoxyglucose-PET imaging. Single slice [^{1}H]MRS imaging was carried out at 1.5 T.

Results: There was a marked reduction in NAA signal intensity in the diaschitic cerebellar hemisphere but minimal reduction in choline and creatine signal intensities. The decrease in NAA signal intensity was most marked in the middle cerebellar peduncle and white matter of the diaschitic cerebellar hemisphere. In the normal subjects and in the uninvolved cerebellar hemisphere of the patient the NAA signal intensity was more prominent in the white matter than the cerebellar cortex.

Conclusion: Our data indicate (a) transneuronal metabolic effects can be detected with [^{1}H]MRS imaging and (b) there is a differential distribution of metabolite signal intensities in the cerebellum with NAA signal intensity predominantly localized to axons of the cerebellar fiber tracts rather than neuronal cell bodies in the cortex and the converse is true for choline and creatine signal intensities.

Index Terms: Cerebellum—Diaschisis—Magnetic resonance spectroscopy—Proton magnetic resonance imaging.

In vivo metabolic imaging of the human CNS until recently was the domain of positron emission tomography (PET) and single photon emission CT (SPECT), but with the development of techniques such as ^{1}H and ^{31}P magnetic resonance spectroscopy (MRS), cerebral metabolites can be assessed with nuclear MR (1–9). Spectroscopic imaging methods are a further advance because they allow simultaneous acquisition of spectra from a large number of voxels within a tissue section. These spectra may be displayed in a tomographic format to depict the regional distributions of metabolite signal intensities. We recently reported the distribution and alterations in the four common metabolite signal intensities [N-acetyl-aspartate (NAA); choline-containing compounds—choline; creatine/phosphocreatine—Cre and lactate], which are identified with [^{1}H]MRS imaging in a large number of patients with brain tumors (10).

From the Neuroimaging Branch (M. J. Fulham, M. J. Dietz, J. R. Alger, and G. Di Chiro), and the National Institute of Neurological Diseases and Stroke, Laboratory of Diagnostic Radiology Research (M. J. Dietz, J. H. Duyn, and H. H.-L. Shih), National Institutes of Health, Bethesda, MD. Dr. M. J. Fulham's present address is the National PET Center, Royal Prince Alfred Hospital, Sydney, Australia. Address correspondence and reprint requests to Dr. G. Di Chiro at Neuroimaging Branch, The Warren G. Magnuson Clinical Center, Building 10, Room 1C453, National Institutes of Health, Bethesda, MD 20892, U.S.A.

Our aims in this study were (a) to determine if the metabolic asymmetry of cerebellar diaschisis which is detected with PET (11–16) is associated with alterations in metabolite signal intensities on [^{1}H]MRS imaging in a patient with documented long-standing cerebellar diaschisis, and (b) to examine the distribution of cerebellar metabolite signals in normal subjects.

SUBJECTS AND METHODS

All subjects were studied under protocols approved by committees of the National Institute of Neurological Diseases and Stroke at the National Institutes of Health (NIH). Informed consent was obtained from each subject before participation in the studies.

Clinical Data

The patient was a 38-year-old right-handed man who developed CNS and retinal toxicity after intra-arterial chemotherapy for a malignant glioma. A left frontal lobe glioblastoma multiforme was diagnosed in the fall of 1988 after a short history of severe unaccustomed headache. Partial resection of the tumor was performed in December 1988 and the patient was referred for participation in an experimental chemotherapy protocol at the NIH. Neurological examination was normal prior to entry into the protocol. The treatment protocol comprised six courses of 1,3-bis(2-chloroethyl)-1-nitrosurea (BCNU) at a dosage of 200 mg/m^2. The BCNU (100 mg) was dissolved in 3 ml of ethanol and diluted in a volume of 140 ml of normal saline and injected into the internal carotid artery on the side of the tumor during diastole. The first course of treatment was given in early February 1989 without incident. Prior to the third treatment in May 1989 a mild expressive dysphasia and a cotton wool spot in the left fundus were noted. On MRI after intravenous gadolinium-diethylenetriamine pentaacetic acid (Gd-DTPA), an increase in enhancement in the left frontal lobe was seen when compared with the earlier studies. The change was interpreted as evidence of tumor progression and so the third treatment was carried out as planned. Ten days later there was the gradual onset, over hours, of right-sided weakness, loss of vision in the left eye, and dysphasia. Treatment with high dose corticosteroids and intravenous heparin was begun but despite these therapies 2 days after the onset of symptoms there was a dense right hemiplegia and aphasia. A fluorodeoxyglucose (FDG)-PET scan carried out 4 days after the development of symptoms showed a reduction in glucose metabolism throughout the left cerebral hemisphere and crossed cerebellar hypometabolism (diaschisis).

Despite extensive rehabilitation there was minimal improvement. The patient is presently able to walk but has a useless right arm and a severe aphasia. He has been followed with regular MR and FDG-PET imaging studies at the NIH since entry into the protocol. There is no evidence of tumor recurrence in the left frontal lobe 4 years after diagnosis but there has been persistent right cerebellar diaschisis on FDG-PET and progressive development of left cerebral hemispheric atrophy (Fig. 1). Although [^{1}H]MRS imaging has been available at our institution since mid-1991, it was not performed on this man until November 1992, together with MR and FDG-PET imaging, 3½ years after the onset of hemiplegia.

[^{1}H]MRS imaging was also done in seven normal subjects: three men and four women aged 25–41 years old with an average age 32 years. All but one subject, a 41-year-old woman, were right handed.

MR Imaging

Spectroscopic data were collected using a GE Signa MR unit (General Electric Medical Systems, Milwaukee, WI, U.S.A.) at 1.5 T equipped with shielded gradients and a quadrature head coil and a point-resolved spectroscopy-chemical shift imaging pulse sequence at echo time (TE) of 272 ms which was developed at the NIH by Moonen et al. (8). This sequence has been reported in detail previously and is only briefly outlined here. A 15 mm axial (z axis) section was selected by the pulse sequence, with slice selection in the anteroposterior and left–right dimensions. Phase-encoding gradient pulses (17–19) allowed the determination of the location of the signal sources within the axial plane. Phase encoding was performed with a resolution of 32 × 32 over a field of view of 24 cm. The sequence ultimately yielded an array of 1,024 [^{1}H]spectra from the plane of the selected tissue section. The resolution, defined as section thickness times (field of view/resolution)^2, from which the spectra arose was 0.8 cm^3. The water signal was suppressed prior to the localization pulses using frequency-selective radiofrequency pulses and gradient pulses (20).

Gradient-echo [MPGR, repetition time (TR) 600, TE 30, 10° flip angle] MRI data were collected after the patient was placed in the MR unit to aid in prescribing the [^{1}H]MRS imaging parameters. Figure 2a and c shows the typical site for the [^{1}H]MRS imaging acquisition in the posterior fossa. The chosen tissue slab was rectangular in shape and was positioned to (a) minimize lipid signal from the surrounding bone in the posterior fossa and (b) include the middle cerebellar peduncles (MCPs) and fourth ventricle in the middle part of the 15 mm tissue

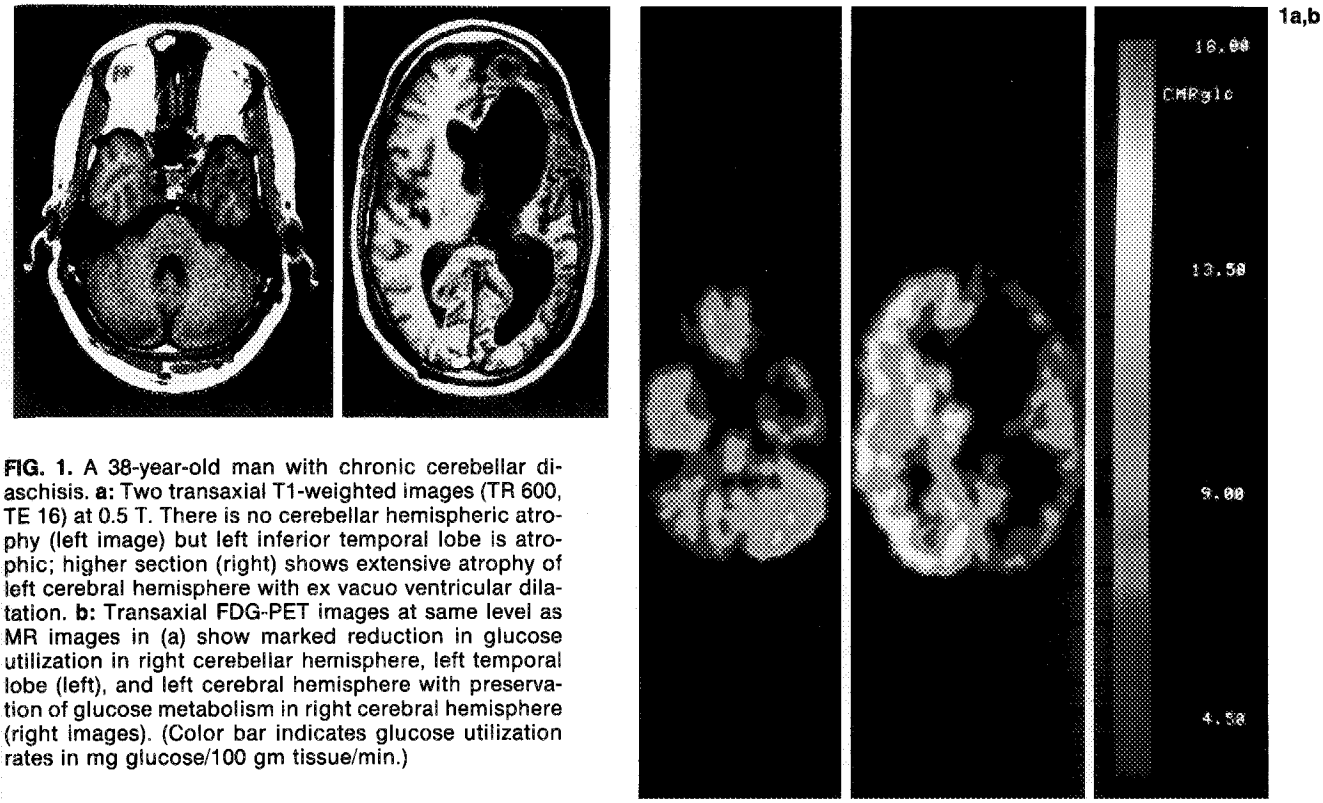

FIG. 1. A 38-year-old man with chronic cerebellar diaschisis. **a:** Two transaxial T1-weighted images (TR 600, TE 16) at 0.5 T. There is no cerebellar hemispheric atrophy (left image) but left inferior temporal lobe is atrophic; higher section (right) shows extensive atrophy of left cerebral hemisphere with ex vacuo ventricular dilatation. **b:** Transaxial FDG-PET images at same level as MR images in (a) show marked reduction in glucose utilization in right cerebellar hemisphere, left temporal lobe (left), and left cerebral hemisphere with preservation of glucose metabolism in right cerebral hemisphere (right images). (Color bar indicates glucose utilization rates in mg glucose/100 gm tissue/min.)

section. The static (B_0) field homogeneity over the chosen tissue slab was adjusted with an automated routine provided in the Signa research package. The spectroscopic data were collected using a TR of 2,000 ms and one acquisition per phase encode step (34.1 min acquisition time). T1-weighted and T2-weighted axial tissue sections from the chosen tissue section were also acquired for both patient and normal subjects.

Clinical MRI T1-weighted (TR 600, TE 16), T2-weighted (TR 2,583, TE 40/100), and T1-weighted sequences after (0.1 mmol/kg) intravenous Gd-DTPA (Magnevist, Berlex Laboratories, Cedar Knolls, NJ, U.S.A.) were also performed in the patient at 0.5 T (Picker Vista HP, Highland Heights, OH, U.S.A.). The study was done, with the orientation of the sections in the same plane as the PET studies, at a second appointment, at least 72 h prior to the [^{1}H]MRS imaging study.

Spectroscopic Data Processing

Raw spectroscopy data were reconstructed on a SUN workstation (SUN Microsystems, CA, U.S.A.) using software developed at our institution. The *k*-space data array was baseline corrected and the spatial *k*-space domain was filtered using a sine-bell function. A two-dimensional Fourier transform was applied to the spatial domain to produce a 32 × 32 array containing the time domain data from the voxels. Residual water signals were filtered from these time domain data using a previously described algorithm (21,22). Zero filling the time domain in each element to 2,048 points and Fourier transformation yielded a 32 × 32 array of spectra. Further analysis was performed on magnitude corrected spectral data. It was necessary to bring the frequency axes of the various spectra into registration because of static (B_0) field variation over the imaged region. This was done using a combination of automated and interactive algorithms for identifying the location of the NAA, choline, or other signals in the relevant spectra. Spectra in which these signals could not be identified (e.g., outside the selected volume and voxels located on or near the skull surface) were nulled so that these data did not appear in the final spectroscopic image. In each remaining spectrum the magnitude of the signal strength within 0.1 ppm on each side of the choline, creatine, NAA, and lactate signal positions was integrated to produce four 32 × 32 arrays showing spatial variation of the strengths of the signals in these regions. These metabolite maps were transferred to a Macintosh computer where they were subjected to further region of interest (ROI) analysis using software developed at the NIH (MacSIMAP v1.1.7). The MPGR, T1-, and T2-weighted image sections were also imported into this environment for anatomical correlation of the [^{1}H]MRS imaging data.

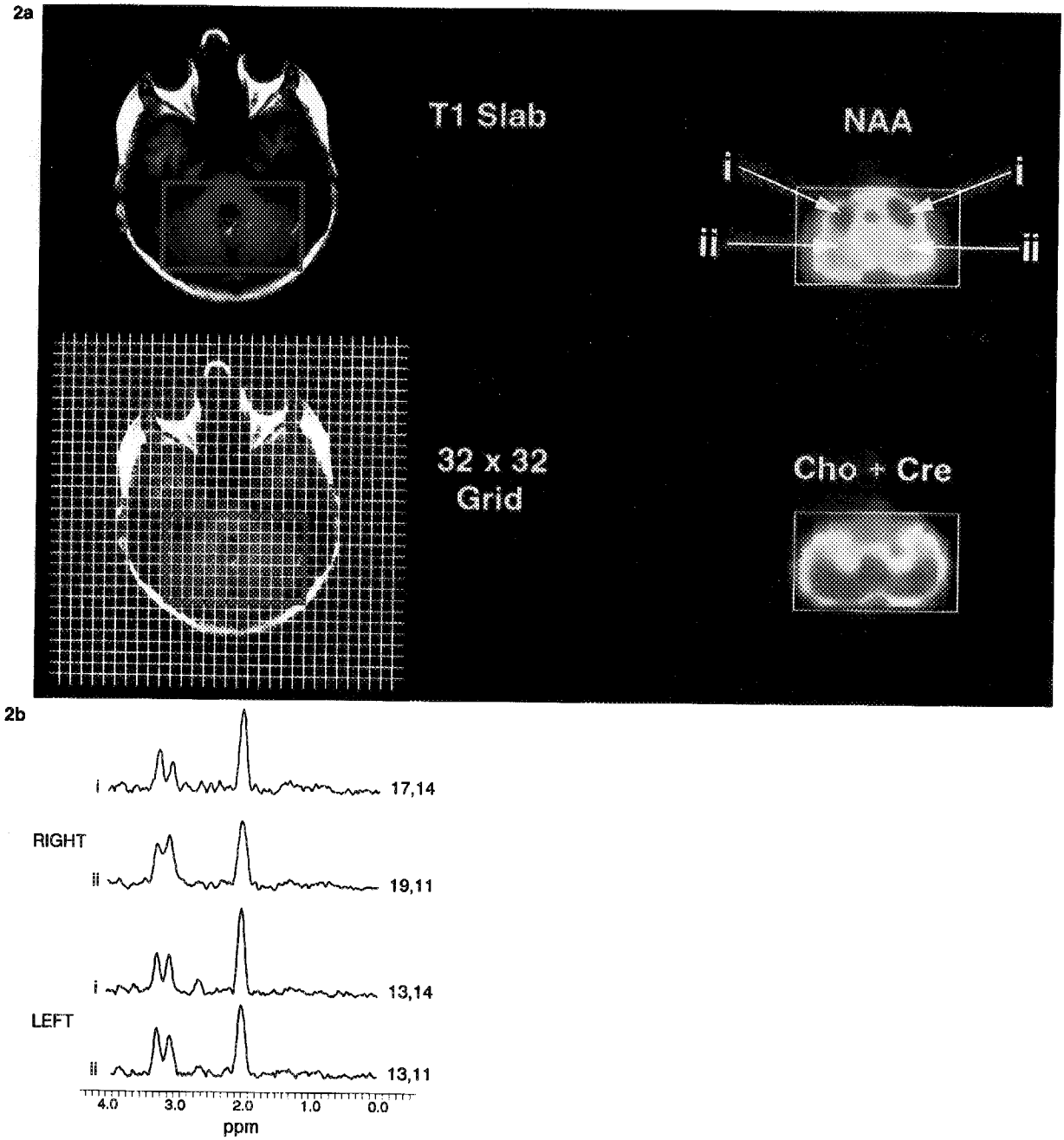

FIG. 2. Metabolite maps and representative spectra for a normal volunteer and patient. Spectra are from single voxels (7 × 7 × 15 mm) from two locations in each cerebellar hemisphere and are indicated by arrows in (a). Location (i) is middle cerebellar peduncle (MCP) adjacent to fourth ventricle, location (ii) is white matter of cerebellar hemisphere. **a:** A 32-year-old right-handed normal woman. (Note for both normal volunteer and patient studies shown here, the posterior fossa regions studied are indicated by rectangular box overlaid onto T1-weighted image and metabolite maps. Rectangular volume of interest in relation to the 32 × 32 grid is also shown. Regions of highest metabolite concentrations appear red and lowest concentrations are green-blue.) T1 image shows that part of pons, fourth ventricle, MCPs, and cerebellar hemispheres are included in metabolite data sets. The NAA metabolite map shows prominent NAA signal in region of MCPs adjacent to signal void from fourth ventricle with lower NAA signals from white matter and cerebellar hemispheres. For choline plus creatine (cho + cre) map, higher metabolite concentrations are seen in region of cerebellar hemispheres with lower signal concentrations in white matter and MCPs. **b:** Normal volunteer in (a). Note in spectrum from right cerebellar white matter (right ii) the choline and creatine signal intensities are not as clearly separated from each other as in the three other spectra shown for this study. **c:** Metabolite maps for patient. There is marked reduction in NAA signal intensity in right cerebellar hemisphere but relative preservation of NAA signal intensity in left MCP and white matter. Minimal asymmetry between diaschitic (right) and uninvolved hemisphere (left) for cho + cre signal intensities is apparent. **d:** Spectra from patient. Locations are identical to those in normal volunteer.

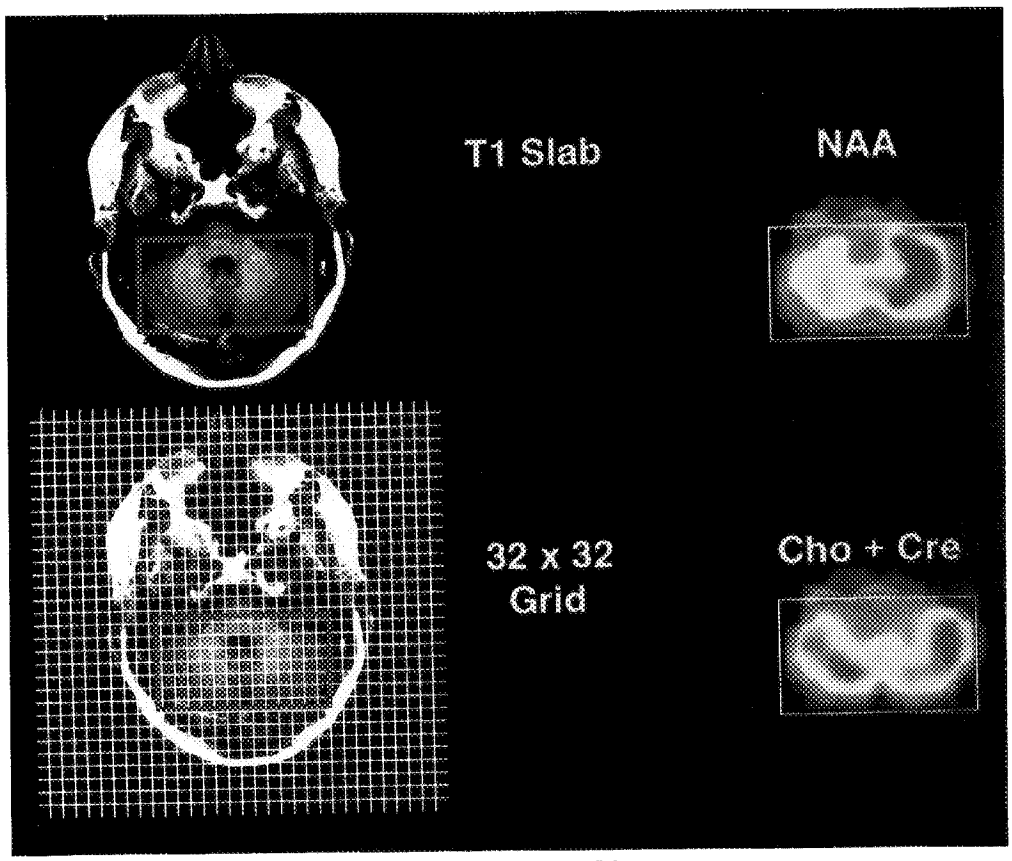

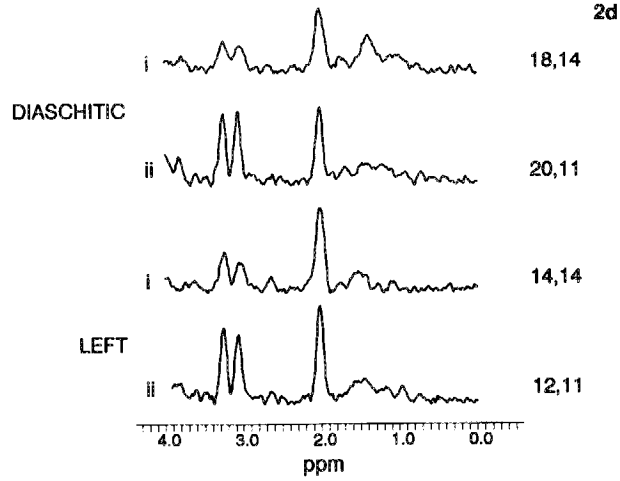

FIG. 2. *Continued.*

The metabolite maps were analyzed qualitatively and quantitatively. In the patient the cerebellar hemisphere opposite the supratentorial lesion was regarded as the diaschitic hemisphere. Metabolite signal amplitudes of the diaschitic hemisphere were compared with the opposite cerebellar hemisphere. The same procedure was carried out for the normal subjects and the left hemisphere was compared with the right cerebellar hemisphere. In these posterior fossa data sets the choline and creatine peaks, in some instances, were broad due to the limited B_0 inhomogeneity characteristics of the posterior fossa and could not be clearly separated from each other in every case (Fig. 2b). The choline and creatine signal intensities were therefore summed for each study. Thus, choline plus creatine signal intensities on the left were compared with those on the right. Quantitative data were obtained by the placement of a large (5 × 7 voxels) rectangular ROI in each cerebellar hemisphere to include the MCP and cer-

ebellar cortex, and an identical ROI was positioned in the corresponding location in the opposite hemisphere.

Finally, the metabolite maps were interpolated to 256 × 256 and smoothed using MacSIMAP for presentation as illustrations in this paper.

FDG-PET

The FDG-PET studies were performed on a Scanditronix PC 2048–15B (SC2) (Scanditronix, Uppsala, Sweden) 15 section tomograph with 6 mm in-plane resolution and 6 mm section thickness. Transmission scans were done to measure attenuation. Our FDG-PET technique has been described in detail elsewhere (16). Patients are fasted for at least 6 h before the study. During the study, blood is sampled from an arterial catheter placed in the radial artery at the wrist. A dose of FDG (185 MBq) is injected via a peripheral intravenous line in the opposite arm while the subject lies in a dimly lit room. The patient's head is immobilized by a thermoplastic mask molded to the contours of the head. The scanning plane is parallel to the canthomeatal line and throughout the examination the patient's eyes and ears are patched. Emission data are acquired after a 30 min uptake period. Glucose metabolic rates were calculated using a modification (23) of the Sokoloff three-compartment model (24) and the gray matter rate constants k_1 0.1020, k_2 0.1300, k_3 0.0620, and k_4 0.0068. The lumped constant value was 0.418. Measurements of glucose utilization in posterior fossa structures were performed using a method and template described in an earlier study (16).

RESULTS

Imaging studies for the patient are shown in Figs. 1 and 2. Magnetic resonance imaging shows extensive left cerebral hemispheric atrophy but without crossed cerebellar atrophy. On FDG-PET there is a marked reduction in glucose utilization in the left cerebral and the right cerebellar hemisphere.

Metabolite maps and representative spectra for a normal right-handed woman and the patient are shown in Fig. 2. Qualitative assessment of the metabolite maps of the normal subjects showed that the distribution of NAA differed from that of choline and creatine. N-Acetyl-aspartate was more prominent in the MCPs and white matter than in the more peripheral cerebellar cortex (Fig. 2a). For choline and creatine maps, signal intensities were more prominent in the cerebellar cortex, seen as a rim around the cerebellar hemispheres and in the vermis, and less obvious in the MCPs and white matter. In the region of the fourth ventricle signal intensities were absent. Although the dentate nuclei are easily seen with FDG-PET on [^{1}H]MRS imaging, these nuclei were not identified. Lactate was not detected in the cerebellar hemispheres or fourth ventricles in either the patient or normal subjects.

A scatter plot of normalized values for NAA and choline plus creatine signals for the patient and normal subjects is shown in Fig. 3. In the normal subjects for NAA, left hemisphere values were less than right in all but one case where the left–right ratio was 1.04. For choline plus creatine, left hemisphere values were also lower than right hemisphere except for one subject where the ratio was 1.04. This was not the same subject as for NAA and both subjects were right handed. For the patient, reductions in NAA in the diaschitic cerebellar hemisphere compared with the normal side was 20.3%; for choline plus creatine there was only a 3% reduction in the diaschitic hemisphere but this reduction was within the ratios seen for the normal subjects.

Glucose utilization rate (GUR), in mg glucose/100 g tissue/min, for the patient in the diaschitic cerebellar cortex was 6.55 compared with 10.18 in the normal or uninvolved hemisphere, which is a 36% reduction. In the cerebellar vermis GUR was 8.13. Although the normal subjects in this study did not have FDG-PET performed, we have previously reported a left–right asymmetry of 1% in 22 normal volunteers using the same methodology and PET scanner (16).

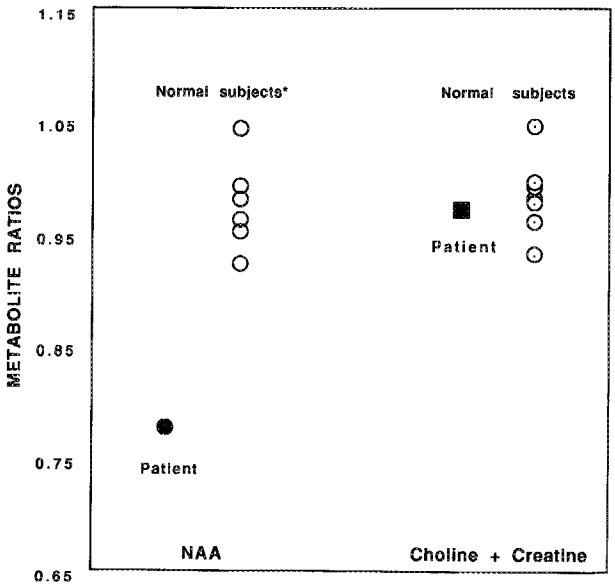

FIG. 3. Scatter plot of N-acetyl-aspartate (NAA) and choline + creatine values for the patient and normal subjects. For normal subjects, left cerebellar hemisphere values are normalized to right cerebellar hemisphere. For the patient, the diaschitic cerebellar hemisphere is normalized to the uninvolved hemisphere. *Two normal subjects had identical values (0.93) for left–right NAA ratio, thus the appearance of only six values.

DISCUSSION

Our main findings are (a) in a patient with a 3 year history of cerebellar diaschisis secondary to cerebral hemispheric chemonecrosis there was a marked reduction in NAA signal intensity but only minimal reduction in creatine and choline signal intensities in the diaschitic cerebellar hemisphere. (b) In normal subjects, NAA signal intensity is more prominent in the MCPs and white matter of the cerebellum rather than in the cerebellar cortex or vermis and the converse is true for choline and creatine signal intensities.

In 1980 Baron et al. (11) were the first to describe a reduction in cerebellar blood flow and metabolism contralateral to supratentorial infarctions using [^{15}O]PET and they called the phenomenon "crossed cerebellar diaschisis." Many PET investigators have since corroborated this work for blood flow, oxygen metabolism, and glucose utilization (13–16). Baron et al. postulated that the likely mechanism for their observation was a transneuronal metabolic depression due to interruption of the corticopontocerebellar tract (CPC) (11). Recent work in brain tumor patients with cerebellar diaschisis showed that there is relative glucose hypometabolism in the brain stem ipsilateral to the tumor at the site of the first CPC synapse (16) and further supports this hypothesis. Early studies suggested that NAA is localized to neurons (25,26) and recently this has been confirmed (27). We therefore hypothesize that (a) the loss of afferent input to the second order neuron in the CPC has resulted in a transneuronal reduction in the NAA signal in the diaschitic cerebellar hemisphere. We believe that ours is the first in vivo demonstration in humans of a transsynaptic effect detected with [^{1}H]MRS imaging. Although the data have only appeared in abstract form, the in vitro spectroscopic work of Rango et al. provide further support for our study (28). They were able to demonstrate a reduction in NAA/creatine ratios in contralateral lateral geniculate body and superior colliculus nuclei 72 h after a stretch injury to guinea pig optic nerve. (b) N-Acetyl-aspartate is more heavily concentrated in the axon of the neuron than the soma.

The cerebellar white matter consists of fibers: (a) association fibers that connect regions within the cerebellum, (b) projection fibers in the cerebellar peduncles, and (c) axons of the Purkinje cells (29). The largest projection fiber tract is the MCP and it contains afferent (mossy) fibers, which arise from contralateral pontine nuclei as the second order neurons in the CPC. The mossy fibers end in synapses in the cerebellar cortex (30). Baron et al. (11) also suggested that the cerebellar asymmetry may be the metabolic correlate of crossed cerebellar atrophy (CCA) (31,32). Although this hypothesis remains unproven, it raises the question: "Could our findings be due to partial volume effects and CCA in the diaschitic cerebellar hemisphere?" We believe this is not the case because in our patient CCA was not seen on MRI (Fig. 1); however, it does not discount that CCA may develop in this man in the future. Tien and Ashdown recently reported that in 8 of 26 patients with cerebellar diaschisis seen on FDG-PET imaging there was evidence of atrophy in the diaschitic hemisphere on MRI at 1.5 T (33). The illness duration for their patients with atrophy was relatively long and ranged from 6 to 15 years (average 9.5 years), and all patients had marked contralateral supratentorial hemispheric atrophy. Such profiles are consistent with neuropathological data (31,32) where CCA is a rare finding and appears to develop many years after a unilateral cerebral injury. However, Tien and Ashdown do not address the issue of cause and effect because their patients were not studied longitudinally with FDG-PET imaging from the onset of the cerebral injury and so the asymmetry in glucose utilization in the eight cases they report might in fact be due to partial volume effects (33).

The choline signal intensity is thought to include contributions from glycerophosphocholine, phosphocholine, and possibly phosphatidylcholine, which are components of phospholipid metabolism and well represented in cell membranes (26,34). The creatine signal intensity includes creatine and phosphocreatine and is important in cell energetics (26,34). Therefore, it is not surprising that the distribution of choline plus creatine signal intensities shows clear localization to the densely cellular cerebellar gray matter of the hemisphere and vermis (Fig. 2) for the patient and normal subjects. Frahm et al. reported regional findings in normal subjects using localized volume techniques in the insula, occipital lobe, thalamus, and cerebellum (35). They found regional differences for NAA signal intensities between gray and white matter areas (higher concentrations) and thalamus and cerebellum (lower concentrations). But they did not find major differences between gray (insula) and white matter (occipital lobe) regions or regional differences for choline and creatine signal intensities between the same areas. However, their study was compromised because of the partial volume errors encountered using MRS and large volumes of interest.

Although there was left–right asymmetry for choline plus creatine signal intensities as well as for NAA metabolite signals in the majority of normal subjects the number of normal subjects is small and we hesitate to draw inferences from this small sample. However, a striking observation is the obvious disparity between the reduction in NAA signal intensity and relative preservation of choline and creatine signal intensities in the diaschitic hemisphere of the patient. The reason for this is unclear but possible explanations include (a) The cerebellar

cortex is not atrophic, i.e., there is no transneuronal degeneration of the third order neurons of the CPC and the cellularity of the cortex is unchanged. (b) Choline and creatine signal intensities are independent of afferent input. It is possible that a reduction in either metabolite might have been masked because we were forced to sum the choline and creatine peaks. The posterior fossa remains a difficult region to study with [^{1}H]MRS imaging; the broadening of the choline and creatine peaks (Fig. 2b and c) in some of the studies would have introduced errors if the metabolites were measured individually with the choline signal partially contaminating the creatine signal and vice versa. We thus chose to sacrifice specificity by summing the peaks. The application of curve-fitting algorithms may help resolve this problem but technical limitations prohibited their implementation for this study (36).

REFERENCES

1. Weiner MW. The promise of magnetic resonance spectroscopy for medical diagnosis. *Invest Radiol* 1988;23:253–61.
2. Bruhn H, Frahm J, Gyngell ML, et al. Cerebral metabolism in man after acute stroke: new observations using localized proton NMR spectroscopy. *Magn Reson Med* 1989;9:126–31.
3. Bruhn H, Frahm J, Gyngell ML, et al. Noninvasive differentiation of tumors with use of localised H-1 MR spectroscopy in vivo: initial experience in patients with cerebral tumors. *Radiology* 1989;172:541–8.
4. Frahm J, Michaelis T, Merboldt K-D, et al. Localized NMR spectroscopy in vivo. Progress and problems. *NMR Biomed* 1989;2:188–95.
5. Segebarth CM, Baleriaux D, De Beer R, et al. 1H Image-guided localized 31P MR spectroscopy of human brain: quantitative analysis of 31P MR spectra measured on volunteers and on intracranial tumor patients. *Magn Reson Med* 1989;11:349–66.
6. Alger JR, Frank JA, Bizzi A, et al. Metabolism of human gliomas: assessment with H-1 MR spectroscopy and F-18 fluorodeoxyglucose PET. *Radiology* 1990;177:633–41.
7. Hubesch B, Sappey-Marinier D, Roth K, Meyerhoff DJ, Matson GB, Weiner MW. P-31 MR spectroscopy of normal human brain and brain tumors. *Radiology* 1990;174:401–9.
8. Moonen CTW, Sobering G, van Zijl PCM, Gillen J, von Keinlin M, Bizzi A. Proton spectroscopic imaging of human brain. *J Magn Reson* 1992;98:556–75.
9. Prichard JW, Brass LM. New anatomical and functional imaging methods. *Ann Neurol* 1992;32:395–400.
10. Fulham MJ, Bizzi A, Deitz MJ, et al. Metabolite mapping of brain tumors with proton MR spectroscopic imaging: clinical relevance. *Radiology* 1992;185:675–86.
11. Baron JC, Bousser MG, Comar D, Castaigne P. Crossed cerebellar diaschisis in human supratentorial infarction [Abstract]. *Ann Neurol* 1980;8:128.
12. Lenzi GL, Frackowiak RSJ, Jones T. Cerebral oxygen metabolism and blood flow in human cerebral infarction. *J Cereb Blood Flow Metab* 1982;2:321–35.
13. Martin WRW, Raichle ME. Cerebellar blood flow and metabolism in cerebral hemisphere infarction. *Ann Neurol* 1983;14:168–76.
14. Kushner M, Alavi A, Reivich M, Dann R, Burke A, Robinson G. Contralateral cerebellar hypometabolism following cerebral insult: a positron emission tomographic study. *Ann Neurol* 1984;15:425–34.
15. Patronas NJ, Di Chiro G, Smith BH, et al. Depressed cerebellar glucose metabolism in supratentorial tumors. *Brain Res* 1984;291:93–101.
16. Fulham MJ, Brooks RA, Hallett M, Di Chiro G. Cerebellar diaschisis revisited: pontine hypometabolism and dentate sparing. *Neurology* 1992;42:2267–73.
17. Kumar A, Welti D, Ernst RR. NMR Fourier zeugmatography. *J Magn Reson* 1975;18:69–83.
18. Brown TR, Kincaid BM, Ugurbil K. NMR chemical shift imaging in three dimensions. *Proc Natl Acad Sci USA* 1982; 79:3523–6.
19. Maudsley AA, Hilal SK, Perman WH, Simon HE. Spatially resolved high resolution spectroscopy by "four dimensional" NMR. *J Magn Reson* 1983;51:147–52.
20. Moonen CTW, van Zijl PCM. Highly effective water suppression for in vivo proton NMR spectroscopy (DRY STEAM). *J Magn Reson* 1990;88:28–41.
21. Marion D, Ikura M, Bax A. Improved solvent suppression in one- and two-dimensional NMR spectra by convolution of time-domain data. *J Magn Reson* 1989;84:425–30.
22. Sobering G, von Kienlin M, Moonen C, van Zijl P, Bizzi A. Post acquisition reduction of water signals in proton spectroscopic imaging of the brain [Abstract]. In: *10th Annual Meeting of the Society of Magnetic Resonance Medicine* 1991:771.
23. Brooks RA. Alternate formula for glucose utilization using labeled deoxyglucose. *J Nucl Med* 1982;23:538–9.
24. Sokoloff L, Reivich M, Kennedy C, et al. The 14C-deoxyglucose method for the measurement of local cerebral glucose utilization: theory procedure and normal values in the conscious and anesthetized albino rat. *J Neurochem* 1977;28:897–916.
25. Birken DL, Oldendorf WH. N-acetyl-L-aspartic acid: a literature review of a compound prominent in 1H-NMR spectroscopic studies of the brain. *Neurosci Biobehav Rev* 1989; 13:23–31.
26. Miller BL. A review of chemical issues in 1H NMR spectroscopy: N-acetyl-l-aspartate, creatine and choline. *NMR Biomed* 1991;4:47–52.
27. Simmons ML, Frondoza CG, Coyle JT. Immunocytochemical localization of N-acetyl-aspartate with monoclonal antibodies. *Neuroscience* 1991;45:37–45.
28. Rango M, Greco F, Tomei G, et al. Trans-synaptic degeneration following acute axonal injury: a 1-H magnetic resonance spectroscopy study. *Neurology* [Abstract]. 1992;42(Suppl 3):475.
29. Williams PL, Warwick R, Dyson M, Bannister LH. Neurology. In: *Gray's Anatomy*. 37th ed. London: Churchill Livingstone, 1989:962–79.
30. Brodal A. The cerebellum. In: *Neurological anatomy in relation to clinical medicine*. New York: Oxford University Press, 1981:294–391.
31. Strefling AM, Urich H. Crossed cerebellar atrophy: an old problem revisited. *Acta Neuropathol (Berl)* 1982;57:197–202.
32. Baudrimont M, Gray F, Meininger V, et al. Atrophie cerebelleuse croisee apres lesion hemispherique survenue a l'age adulte. *Rev Neurol (Paris)* 1983;139:485–95.
33. Tien RD, Ashdown BC. Crossed cerebellar diaschisis and crossed cerebellar atrophy: correlation of MR findings, clinical symptoms, and supratentorial diseases in 26 patients. *AJR* 1991;158:1155–9.
34. Agris PF, Campbell ID. Proton nuclear magnetic resonance of intact Freund leukemia cells: phosphorylcholine increase during differentiation. *Science* 1982;216:1325–7.
35. Frahm J, Bruhn H, Gyngell ML, Merboldt KD, Hanicke W, Sauter R. Localized proton NMR spectroscopy in different regions of the human brain in vivo. Relaxation times and concentrations of cerebral metabolites. *Magn Reson Med* 1989;11:47–63.
36. Bottomley PA. The trouble with spectroscopy papers. *Radiology* 1991;181:344–50.